

Photoelectron Spectroscopy

Observation of Transition-Metal–Boron Triple Bonds in IrB_2O^- and ReB_2O^-

 Teng-Teng Chen[†], Ling Fung Cheung[†], Wei-Jia Chen, Joseph Cavanagh, and Lai-Sheng Wang*

Abstract: Multiple bonds between boron and transition metals are known in many borylene (:BR) complexes via metal $d_\pi \rightarrow \text{BR}$ back-donation, despite the electron deficiency of boron. An electron-precise metal–boron triple bond was first observed in BiB_2O^- [$\text{Bi}\equiv\text{B}-\text{B}\equiv\text{O}$][−] in which both boron atoms can be viewed as sp -hybridized and the $[\text{B}-\text{BO}]^-$ fragment is isoelectronic to a carbyne (CR). To search for the first electron-precise transition-metal–boron triple-bond species, we have produced IrB_2O^- and ReB_2O^- and investigated them by photoelectron spectroscopy and quantum-chemical calculations. The results allow to elucidate the structures and bonding in the two clusters. We find IrB_2O^- has a closed-shell bent structure (C_s , $^1A'$) with BO^- coordinated to an $\text{Ir}\equiv\text{B}$ unit, $(-\text{OB})\text{Ir}\equiv\text{B}$, whereas ReB_2O^- is linear ($C_{\infty v}$, $^3\Sigma^-$) with an electron-precise $\text{Re}\equiv\text{B}$ triple bond, $[\text{Re}\equiv\text{B}-\text{B}\equiv\text{O}]^-$. The results suggest the intriguing possibility of synthesizing compounds with electron-precise $\text{M}\equiv\text{B}$ triple bonds analogous to classical carbyne systems.

Even though borylenes (:BR) are isoelectronic to CO ,^[1] their chemistry is more analogous to carbenes (:CR_2) and they can form metal–boron multiple bonds because they are much better π -acceptors. The first transition-metal borylene complexes were synthesized in 1998.^[2] Since then, many borylene complexes have been synthesized^[3] and the field has experienced rapid advances.^[4] These compounds usually involve a transition metal with different ligands (L_n), $L_n\text{MBR}$. The bonding between the metal (M) and the borylene fragment is described generally as $\text{B} \rightarrow \text{M}$ σ -donation and $\text{M}(d_\pi) \rightarrow \text{B}$ back-donation.^[5] The analogy of borylenes and carbenes suggests a $\text{M}=\text{B}$ double bond in $L_n\text{M}=\text{BR}$. However, because borylenes are strong π -acceptors, the $\text{M}-\text{B}$ bond length spans a wide range, depending on the ligands on the metal and the R group.^[4a] In fact, a metal–boron triple-bond character was first suggested in the $[(\text{OC})_5\text{Cr}=\text{BSi}(\text{SiMe}_3)_3]$ complex,^[3f] which has a $\text{Cr}-\text{B}$ bond length of 1.878 Å, slightly shorter than the $\text{Cr}=\text{B}$ double-bond length (1.89 Å) predicted from Pyykkö's double-bond covalent radii.^[6] Several transition-metal–borylene complexes feature $\text{M}-\text{B}$ bond lengths shorter than $\text{M}=\text{B}$ double bonds derived from Pyykkö's double-bond

covalent radii.^[3b–h] The shortest metal–boron bond length was reported recently in a $L_n\text{FeBF}$ compound^[7] with an $\text{Fe}-\text{B}$ bond length of 1.7703 Å, which is comparable to the $\text{Fe}\equiv\text{B}$ triple-bond length (1.75 Å) based on Pyykkö's triple-bond covalent radii.^[6] Another recent study on a series of F_2MBF complexes using matrix-isolation infrared spectroscopy and quantum-chemical calculations showed an $\text{M}\equiv\text{B}$ triple-bond character for $\text{M}=\text{Ir}$ and Os with $\text{M}-\text{B}$ bond lengths comparable to those computed from Pyykkö's triple-bond covalent radii.^[8]



If boron acquires an electron, the $[\text{BR}]^-$ unit becomes isoelectronic to a carbyne (CR) unit. Transition-metal complexes of such borylene ligands are not known. The first metal borylene species was observed in BiB_2O^- , which has a linear $[\text{Bi}\equiv\text{B}-\text{B}\equiv\text{O}]^-$ structure with a $\text{Bi}\equiv\text{B}$ triple bond.^[9] Both B atoms are sp -hybridized and BiB_2O^- is an electron-precise molecule. To search for the first transition-metal–borylene complex, we recently examined RhB_2O^- using photoelectron spectroscopy (PES) and theoretical chemistry and found that it does not have the expected linear $[\text{Rh}\equiv\text{B}-\text{B}\equiv\text{O}]^-$ structure.^[10] Instead, it was found to have a bent structure with BO^- coordinated to the Rh atom, which features a very short $\text{Rh}-\text{B}$ bond exhibiting quadruple-bond character, $(-\text{OB})\text{Rh}\equiv\text{B}$. This led to the discovery of the first $\text{Rh}\equiv\text{B}$ quadruple bond in a diatomic molecule involving boron.^[10,11] In the meantime, a combined infrared and theoretical study on $\text{BFe}(\text{CO})_3^-$ showed that B and Fe engage in quadruple bonding,^[12] even though the diatomic FeB has a much weaker bond.^[13]

We have been interested in probing the electronic structure and chemical bonding of size-selected boron clusters^[14] and metal-doped boron clusters^[15] using PES and computational chemistry. The current study continues our quest for the first transition-metal borylene complex. We have produced IrB_2O^- and ReB_2O^- and obtained their PE spectra, which are combined with theoretical calculations to elucidate their structures and bonding. IrB_2O^- is found to adopt a bent structure similar to that of RhB_2O^- , except that the $\text{Ir}-\text{B}$ bonding displays more triple-bond character. ReB_2O^- is found to possess a perfectly linear $[\text{Re}\equiv\text{B}-\text{B}\equiv\text{O}]^-$ structure with a $\text{Re}\equiv\text{B}$ triple bond, which can be viewed as the first transition-metal borylene complex.

The experiments were carried out using a magnetic-bottle PES apparatus coupled with a laser vaporization cluster source (see Supporting Information for more details).^[14f,16] The PE spectra of IrB_2O^- and ReB_2O^- are shown in Figure 1 and 2, respectively. The 355 nm spectrum of IrB_2O^- (Figure 1a) exhibits an intense and sharp ground-state band X, which displays a short vibrational progression with a frequency of 870 cm^{-1} . The 0–0 transition at 2.90 eV yields the adiabatic detachment energy (ADE) of IrB_2O^- , which is also

[*] T. T. Chen,^[†] L. F. Cheung,^[†] W. J. Chen, J. Cavanagh, Prof. Dr. L. S. Wang
Department of Chemistry, Brown University
Providence, RI 02912 (USA)
E-mail: Lai-Sheng_Wang@brown.edu

[†] These authors contributed equally to this work.

 Supporting information and the ORCID identification number(s) for the author(s) of this article can be found under:
 <https://doi.org/10.1002/anie.202006652>.

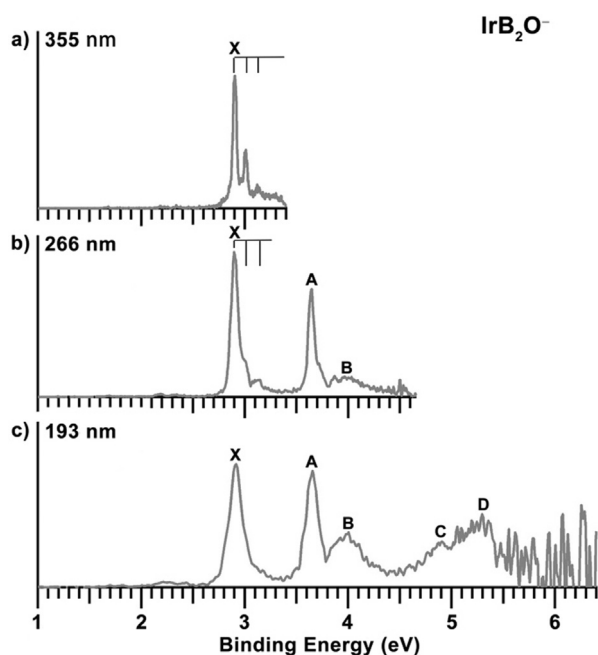


Figure 1. Photoelectron spectra of IrB_2O^- at a) 355 nm (3.496 eV), b) 266 nm (4.661 eV), and c) 193 nm (6.424 eV). The resolved vibrational structures are labeled for bands X and A in (a) and (b).

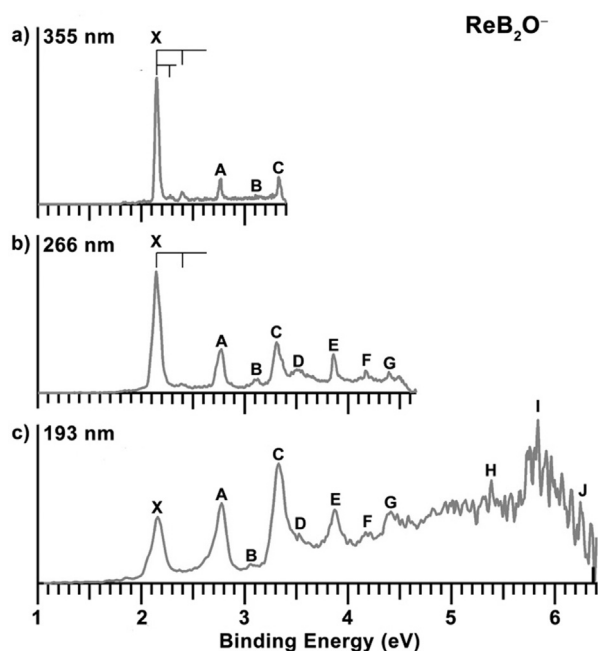


Figure 2. Photoelectron spectra of ReB_2O^- at a) 355 nm, b) 266 nm, and c) 193 nm. The resolved vibrational structures are labeled for band X in (a) and (b).

the electron affinity (EA) of neutral IrB_2O . Following a large energy gap, band A at 3.65 eV in the 266 nm spectrum (Figure 1 b) is also quite intense and sharp, similar to band X. Band B at 3.96 eV in both the 266 nm and 193 nm spectra (Figure 1 c) is broad and weaker than bands X and A. Band C at 4.90 eV and band D at 5.29 eV are broad and not well

resolved. Above 5.5 eV, the signal-to-noise ratios are poor, and no definite spectral transitions can be identified. It should be pointed out that the overall 193 nm spectral pattern of IrB_2O^- shows some similarities to that of the recently reported RhB_2O^- ,^[10] suggesting they may have similar structures.

The spectra of ReB_2O^- (Figure 2) are completely different, displaying a series of sharp spectral features below 4.5 eV. These observations indicate that ReB_2O^- likely has a more symmetric structure and that there is little structural change upon electron detachment. The ground-state band X in the 355 nm spectrum (Figure 2 a) is intense and sharp with two weak vibrational features at 1060 cm^{-1} and 1960 cm^{-1} . Band X yields an EA of 2.15 eV for neutral ReB_2O . Band A at 2.77 eV is sharp with a relatively weak intensity, which increases with the photon energy (Figure 2 b,c). Band B at 3.13 eV is very weak in the 355 nm spectrum and slightly more visible in the 266 nm spectrum (Figure 2 b). Band C at 3.30 eV in the 355 nm spectrum is similar to band A, and its relative intensity increases with photon energies and becomes the most intense peak in the 193 nm spectrum (Figure 2 c). A weak and broad band D at 3.51 eV is observed in the 266 nm spectrum along with three more sharp bands: E at 3.86 eV, F at 4.17 eV, and G at 4.40 eV (Figure 2 b). In the 193 nm spectrum (Figure 2 c), essentially continuous signals are observed above 4.5 eV, and bands H, I, and J are labeled for the sake of discussion. The VDEs of the observed spectral bands are given in Table 1 and 2 for IrB_2O^- and ReB_2O^- , respectively, where they are compared with theoretical data.

To understand the electronic structure and chemical bonding of IrB_2O^- and ReB_2O^- , we carried out theoretical calculations using the TPSSH and CCSD(T) methods.^[17] We used the aug-cc-pVTZ-pp basis set and the relativistic effective core potential ECP60MDF for Re and Ir,^[18] as well as the aug-cc-pVTZ basis set for B and O.^[19] The first VDE was calculated as the energy difference between the anion and neutral at the anion geometry. Higher VDEs were calculated using TD-DFT and the TPSSH functional.^[20] Different structures were computed and those within 1 eV of the global minima are given in Figure S1 (Supporting Information). The global minima of IrB_2O^- and ReB_2O^- calculated using the TPSSH method are shown in Figure 3. We found that the global minimum of IrB_2O^- is a bent structure with a BO^- unit coordinated to the Ir atom, which forms a short Ir–B bond with a terminal B atom, similar to the

Table 1: Comparison of the experimental and theoretical results for IrB_2O^- . The experimental and theoretical VDEs for IrB_2O^- are given in eV. The theoretical VDEs were calculated using the CCSD(T) method for the first VDE and using TD-TPSSH for the higher VDEs.

Peak	VDE (exp.)	VDE (theo.)	Electronic state and MO configuration
X	2.90	3.02	$^2A'$, $1a'^22a'^23a'^24a'^25a'^21a''^22a''^26a'^27a'^23a''^28a'^1$
A	3.65	3.88	$^2A''$, $1a'^22a'^23a'^24a'^25a'^21a''^22a''^26a'^27a'^23a''^18a'^2$
B	3.96	4.23	$^2A'$, $1a'^22a'^23a'^24a'^25a'^21a''^22a''^26a'^27a'^13a''^18a'^2$
C	4.90	4.93	$^2A''$, $1a'^22a'^23a'^24a'^25a'^21a''^22a''^16a'^27a'^23a''^18a'^2$
D	5.29	5.20	$^2A'$, $1a'^22a'^23a'^24a'^25a'^21a''^22a''^26a'^17a'^23a''^18a'^2$
		6.20	$^2A''$, $1a'^22a'^23a'^24a'^25a'^21a''^12a''^16a'^27a'^23a''^18a'^2$

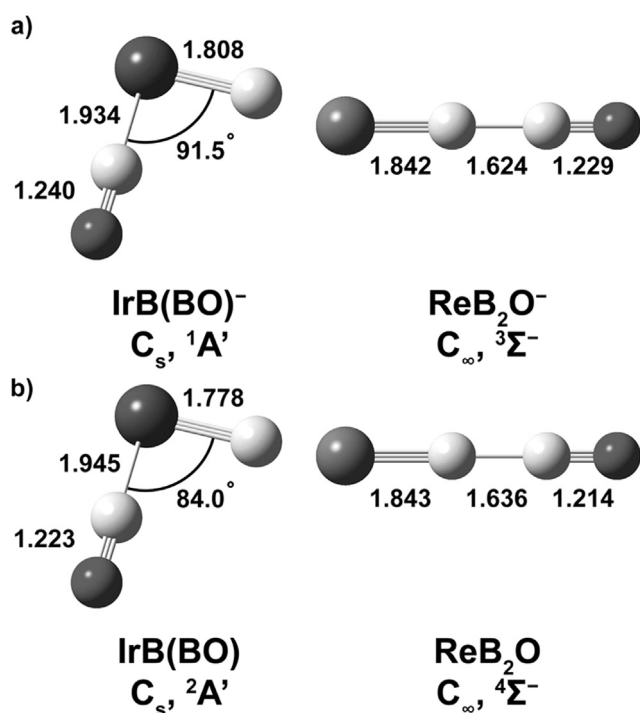


Figure 3. The optimized structures for a) IrB₂O⁻ and ReB₂O⁻ as well as b) IrB₂O and ReB₂O using the TPSSh method. Bond lengths are given in Å.

global minimum of RhB₂O⁻ reported recently.^[10] The linear isomer for IrB₂O⁻ (1Σ⁺) was found to be 0.58 eV higher in energy (Figure S1a). However, we found that the global minimum of ReB₂O⁻ is linear with a short Re–B bond and a BO⁻ unit bonded to the B atom. The second low-lying isomer for ReB₂O⁻ is also linear, but with a higher spin state, which is 0.72 eV above the global minimum (Figure S1b). The molecular orbitals (MOs) of IrB₂O⁻ and ReB₂O⁻ are shown in Figure S2. The normal modes of vibration and their computed frequencies for neutral IrB₂O and ReB₂O are shown in Figure S3. The calculated first VDEs and vibrational frequencies are compared with the experimental results in Table S1.

For IrB₂O⁻, electron detachment from the highest occupied molecular orbital (HOMO) 8a' gives rise to a calculated first VDE at 3.02 eV, where the experimental value is 2.90 eV (Table 1). The computed Ir–B stretching frequency for the short Ir–B bond is 907 cm⁻¹, in reasonable agreement with the experimental result of 870 cm⁻¹. Band A results from electron detachment from the 3a'' orbital with a computed VDE at 3.88 eV, agreeing well with the experimental value at 3.65 eV. Detachment from the 7a' orbital gives a theoretical VDE of 4.23 eV, in good agreement with band B at 3.96 eV, whereas detachment from the 2a'' MO with a computed VDE of 4.93 eV is in excellent agreement with that of band C at 4.90 eV. Band D at 5.29 eV corresponds to detachment from the 6a' orbital with a calculated VDE at 5.20 eV. The 8a' and 3a'' orbitals are nonbonding 5d orbitals (Figure S2), consistent with the sharp PES bands X and A. The PES bands B, C, and D correspond to detachment from the bonding MOs 7a', 2a'', and 6a', respectively, in good agreement with the broad PES

features. Overall, the theoretical data for IrB₂O⁻ are in excellent agreement with the experimental results, unequivocally confirming the bent global minimum.

For ReB₂O⁻, the first electron detachment is from the 5σ orbital, leading to the 4Σ⁻ ground state of neutral ReB₂O. The computed VDE of 1.95 eV was underestimated in comparison to the experimental result at 2.15 eV (Table 2). Very weak vibrational features were resolved in the 355 nm spectrum (Figure 2a) and the two observed vibrational bands at 1060 and 1960 cm⁻¹ agree well with the calculated frequencies for the B–B (ν₂) and B–O (ν₁) stretching modes at 1161 and 2010 cm⁻¹, respectively (Figure S3). The 5σ MO is mainly a nonbonding Re 6s orbital (Figure S2), consistent with the fact that there is little geometry change between the anion and the neutral ground state (Figure 3) and the large detachment cross-section at 355 nm. Detachment from the 5σ MO can also result in a low-spin 2Σ⁻ state with a computed VDE of 3.55 eV, in good agreement with peak D (Table 2). The next detachment channel comes from the 1δ singly occupied molecular orbital (SOMO), which consists purely of the Re 5d_{xy}/5d_{x²-y²} orbitals (Figure S2), resulting in a 2Δ final state. Spin–orbit (SO) splitting leads to two final states (2Δ_{3/2} and 2Δ_{5/2}), which are assigned to peaks A and B. The separation between peaks A and B (2900 cm⁻¹) is consistent with the SO splitting of the Re atom,^[21] and the computed VDE of 2.99 eV (without considering SO effects) is in good agreement with the average VDE of peaks A and B. The atomic-like sharp peak A and the low detachment cross-section at 355 nm are both in perfect accord with the nature of the 1δ MO. The next detachment channel stems from the 2π bonding MO, which can yield two final states: 4Π and 2Π. The computed VDEs of 3.45 eV and 3.89 eV (without SO effects) are in good agreement with the observed VDEs of peaks C and E, respectively (Table 2). However, SO splitting can give rise to multiple final states: 4Π_{5/2,3/2,1/2} and 2Π_{3/2,1/2}, which agree qualitatively with the additional weak features (F and G) and possible unresolved features on the higher-binding-energy side. Additional detachment channels all stem from strongly bonding MOs at higher binding energies, which are expected to yield broad features, consistent with the continuous PES signals on the higher-binding-energy side in the 193 nm spectrum (Fig-

Table 2: Comparison of the experimental and theoretical results for ReB₂O⁻. The experimental and theoretical VDEs for ReB₂O⁻ are given in eV. The theoretical VDEs were calculated using the CCSD(T) method for the first VDE and using TD-TPSSh for the higher VDEs.

Peak	VDE (exp.)	VDE (theo.)	Electronic state and MO configuration
X	2.15	1.95	4Σ ⁻ , 1σ ² 2σ ² 3σ ² 1π ⁴ 4σ ² 2π ⁴ 5σ ¹ 1δ ²
A	2.77	2.99	2Δ _{3/2} , 1σ ² 2σ ² 3σ ² 1π ⁴ 4σ ² 2π ⁴ 5σ ² 1δ ¹
B	3.13		2Δ _{5/2} , 1σ ² 2σ ² 3σ ² 1π ⁴ 4σ ² 2π ⁴ 5σ ² 1δ ¹
C	3.30	3.45	4Π _{5/2} , 1σ ² 2σ ² 3σ ² 1π ⁴ 4σ ² 2π ³ 5σ ² 1δ ²
D	3.51	3.55	2Σ ⁻ , 1σ ² 2σ ² 3σ ² 1π ⁴ 4σ ² 2π ⁴ 5σ ¹ 1δ ²
E	3.86	3.89	2Π _{3/2} , 1σ ² 2σ ² 3σ ² 1π ⁴ 4σ ² 2π ³ 5σ ² 1δ ²
F	4.17		4Π _{3/2} , 1σ ² 2σ ² 3σ ² 1π ⁴ 4σ ² 2π ³ 5σ ² 1δ ²
G	4.40		2Π _{1/2} , 1σ ² 2σ ² 3σ ² 1π ⁴ 4σ ² 2π ³ 5σ ² 1δ ²
H	5.39	5.84	4Π _{1/2} , 1σ ² 2σ ² 3σ ² 1π ⁴ 4σ ² 2π ³ 5σ ² 1δ ²
I	5.85	6.06	2Σ ⁺ , 1σ ² 2σ ² 3σ ² 1π ⁴ 4σ ¹ 2π ⁴ 5σ ² 1δ ²
J	≈ 6.2	6.39	2Π, 1σ ² 2σ ² 3σ ² 1π ³ 4σ ² 2π ⁴ 5σ ² 1δ ²

ure 2c). Overall, the observed spectral pattern of ReB_2O^- agrees well with the theoretical data. Only a linear structure can yield such complicated PE spectra due to the strong SO effects and the resulting different total-angular-momentum states.

In addition to the MO analyses (Figure S2), we also performed chemical-bonding analyses for IrB_2O^- and ReB_2O^- using the adaptive natural density partitioning (AdNDP) method and the TPSSh functional,^[22] as shown in Figure 4. The AdNDP results of IrB_2O^- revealed a $5d_{z^2}$, a $5d_{xz}$, and an O sp lone-pair orbital (first row in Figure 4a) as well as a $\text{B}\equiv\text{O}$ triple bond and an $\text{OB}-\text{Ir}$ single bond (third row). The second row in Figure 4a depicts the bonding between Ir and the terminal B atom, showing an $\text{Ir}\equiv\text{B}$ triple bond and a $\text{B}-\text{Ir}-\text{B}$ three-center ($3c-2e$) bond. The $\text{Ir}-\text{B}$ bond length of 1.808 Å in IrB_2O^- is consistent with the $\text{Ir}\equiv\text{B}$

triple-bond length (1.80 Å) predicted from Pyykkö's covalent atomic radii.^[6] The structure and bonding of IrB_2O^- are similar to RhB_2O^- , which has a $\text{Rh}\equiv\text{B}$ quadruple-bond character.^[10] The difference of bonding in the two isoelectronic systems lies in the $\text{B}-\text{M}-\text{B}$ bond angles and the $3c-2e$ $\text{B}-\text{M}-\text{B}$ bond. The $\text{B}-\text{Rh}-\text{B}$ bond angle is 99.8° and therefore larger than the $\text{B}-\text{Ir}-\text{B}$ bond angle of 91.5° . The smaller bond angle in IrB_2O^- allows a more delocalized $3c-2e$ $\text{B}-\text{Ir}-\text{B}$ bond, whereas in RhB_2O^- , the $3c-2e$ bond is more localized on the terminal $\text{Rh}-\text{B}$ bond, giving rise to its quadruple-bond character. This difference in $\text{M}-\text{B}$ bonding in the MB_2O^- systems is similar to the difference in the diatomic MB systems. While RhB was recently found to possess a quadruple bond,^[10] a very recent study found that IrB actually has a smaller bond order of 3.5.^[23] The difference in bonding between Ir and Rh is due to the relativistic effects that stabilize the 6s orbital in Ir, so that IrB has a triplet ground state ($^3\Delta$) due to the promotion of an electron from a 5d lone-pair orbital to a 6s-dominated, weakly antibonding MO,^[23] whereas RhB is closed shell ($^1\Sigma^+$) because the 5s-dominated LUMO is much higher in energy.^[10] Hence, the bent IrB_2O^- structure can be expressed approximately as $(-\text{OB})\text{Ir}\equiv\text{B}$, while RhB_2O^- can be expressed as $(-\text{OB})\text{Rh}\equiv\text{B}$.

The AdNDP analyses of the linear ReB_2O^- are straightforward (Figure 4b), revealing a $\text{Re}\equiv\text{B}$ triple bond, a $\text{B}\equiv\text{O}$ triple bond, a single $\text{B}-\text{B}$ bond, two unpaired electrons in the $5d_{xy}$ and $5d_{x^2-y^2}$ orbitals, a 6s lone-pair, and an O sp lone-pair orbital. Thus, the linear ReB_2O^- can be expressed as $[\text{Re}\equiv\text{B}-\text{B}\equiv\text{O}]^-$ in which both B atoms are sp-hybridized, similar to carbyne complexes. The $\text{Re}-\text{B}$ bond length of 1.842 Å is in good agreement with the value of 1.83 Å obtained from Pyykkö's triple-bond covalent atomic radii.^[6]

We further analyzed the orbital composition using the natural atomic orbital (NAO) method^[24] to gain more insights into the $\text{M}-\text{B}$ bonding in IrB_2O^- and ReB_2O^- , as shown in Tables S2 and S3, respectively. Because these are relatively simple systems, the MOs exhibit some similarities to the AdNDP results, but the MOs carry information about the detailed atomic compositions, as given in Tables S2

and S3, respectively. Because these are relatively simple systems, the MOs exhibit some similarities to the AdNDP results, but the MOs carry information about the detailed atomic compositions, as given in Tables S2

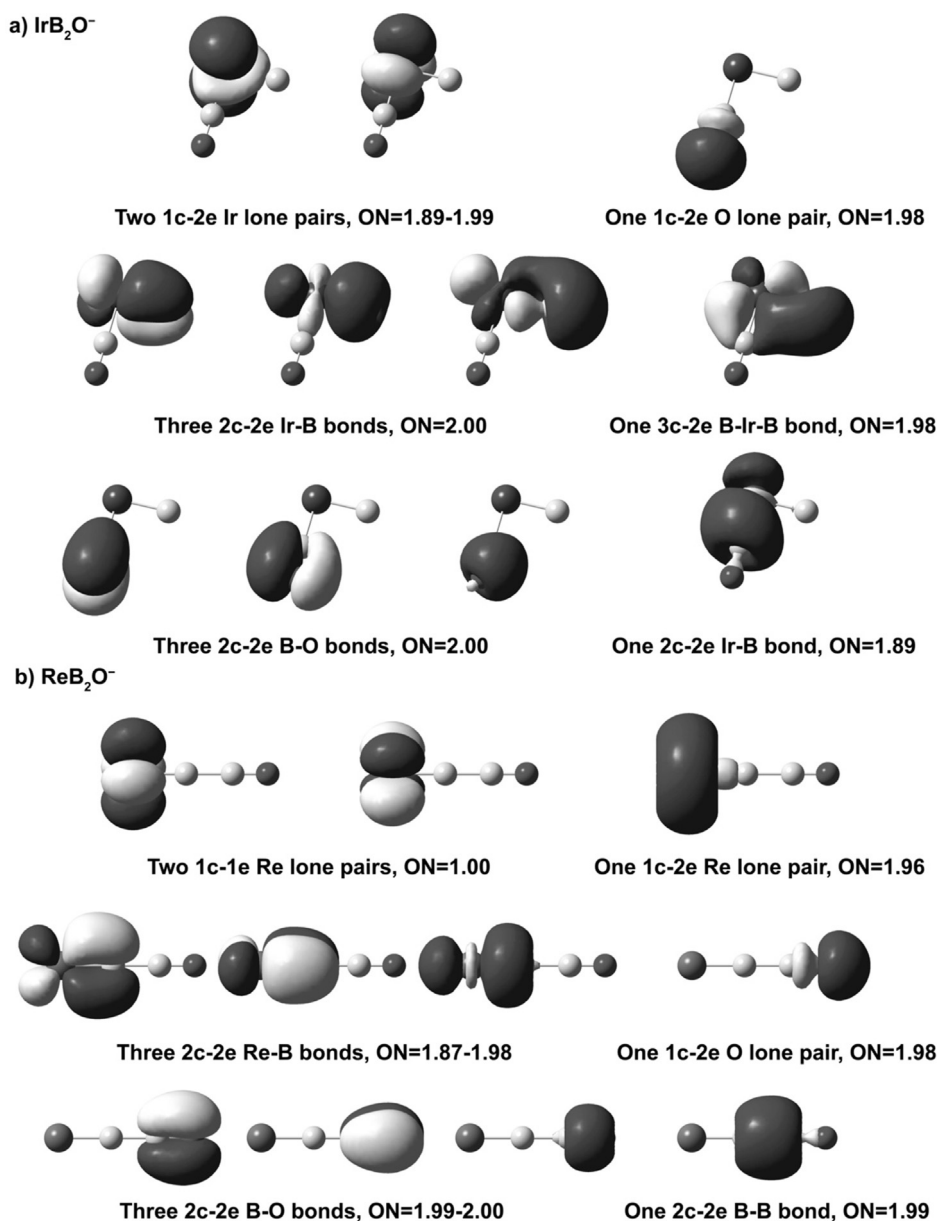


Figure 4. Chemical-bonding analyses using AdNDP for a) IrB_2O^- and b) ReB_2O^- .

and S3. For IrB_2O^- , the HOMO–1 and HOMO–9 represent the Ir–B σ bonds, but the HOMO–9 is clearly a B–Ir–B three-center bond (Figure S2). For ReB_2O^- , the AdNDP results are nearly the same as the MOs (Figure S2, Table S3). We also analyzed the bond order for $\text{IrB}_2\text{O}^{-/0}$ and $\text{ReB}_2\text{O}^{-/0}$ using the Mayer and Nalewajski–Mrozek methods^[25] at PBE/QZ4P^[26] using ADF,^[27] as given in Table S4. Both the Mayer and Nalewajski–Mrozek bond orders for the $\text{Re}\equiv\text{B}$ bond in ReB_2O^- were almost exactly 3 (2.9 and 3.1, respectively). The bond orders computed for the $\text{Ir}\equiv\text{B}$ bond in IrB_2O^- are slightly lower than 3 (2.5 and 2.8, respectively) due to the B–Ir–B three-center bonding.

To understand why the bent structure is preferred over the linear structure for IrB_2O^- , we computed the bond dissociation energies (BDE) of the reaction $\text{IrB}_2\text{O}^- \rightarrow \text{IrB} + \text{BO}^-$ for the bent and linear structures, as shown in Table S5. The larger BDE for the bent structure (8.07 eV) can be attributed to the B–Ir–B three-center bond in the bent structure. The different structures of ReB_2O^- and IrB_2O^- are surprising at first glance, which can be understood by considering the bonding in the linear isomer of IrB_2O^- . From the MOs of the linear ReB_2O^- (Figure S2), we can see that two more electrons in Ir relative to Re would be added to the 1d SOMO to give the closed-shell linear isomer (Figure S1a), resulting in three non-bonding lone-pair orbitals. However, in the bent structure of IrB_2O^- , there are only two non-bonding lone pairs (Figures 4 and S2). It can be assumed that those two additional electrons in fact form the extra 3c–2e B–Ir–B bond in the bent structure, providing the extra stability over the linear isomer.

In conclusion, we report an investigation on the electronic structure and chemical bonding of two transition-metal–boron complexes (IrB_2O^- and ReB_2O^-) using photoelectron spectroscopy and quantum-chemical calculations. Distinct and different spectral features are observed for the two species and are used to compare with theoretical calculations. IrB_2O^- is found to have a bent structure with a BO^- unit coordinated to the Ir atom, whereas ReB_2O^- is found to have a linear structure in which the BO^- unit is bonded to the B atom. Chemical-bonding analyses reveal that both contain an $\text{M}\equiv\text{B}$ triple bond and can be viewed as $(^-\text{OB})\text{Ir}\equiv\text{B}$ and $[\text{Re}\equiv\text{B}-\text{B}\equiv\text{O}]^-$. ReB_2O^- can be considered as the first electron-precise transition-metal borylyne complex.

Acknowledgements

This work was supported by the National Science Foundation (CHE-1763380). The calculations were performed using resources at the Center for Computation and Visualization (CCV) of Brown University.

Conflict of interest

The authors declare no conflict of interest.

Keywords: borylyne · chemical bonding · photoelectron spectroscopy · transition metals · triple bonds

- [1] A. W. Ehlers, E. V. Barends, F. M. Bickelhaupt, U. Radius, *Chem. Eur. J.* **1998**, *4*, 210–221.
- [2] a) H. Braunschweig, C. Kollann, U. Englert, *Angew. Chem. Int. Ed.* **1998**, *37*, 3179–3180; *Angew. Chem.* **1998**, *110*, 3355–3357; b) A. H. Cowley, V. Lomelf, A. Voigt, *J. Am. Chem. Soc.* **1998**, *120*, 6401–6402.
- [3] a) H. Braunschweig, M. Colling, C. Kollann, H. G. Stammer, B. Neumann, *Angew. Chem. Int. Ed.* **2001**, *40*, 2298–2300; *Angew. Chem.* **2001**, *113*, 2359–2361; b) D. L. Coombs, S. Aldridge, C. Jones, D. J. Willock, *J. Am. Chem. Soc.* **2003**, *125*, 6356–6357; c) D. L. Coombs, S. Aldridge, A. Rossin, C. Jones, D. J. Willock, *Organometallics* **2004**, *23*, 2911–2926; d) H. Braunschweig, M. Burzler, T. Kupfer, K. Radacki, F. Seeler, *Angew. Chem. Int. Ed.* **2007**, *46*, 7785–7787; *Angew. Chem.* **2007**, *119*, 7932–7934; e) H. Braunschweig, K. Radacki, K. Uttinger, *Angew. Chem. Int. Ed.* **2007**, *46*, 3979–3982; *Angew. Chem.* **2007**, *119*, 4054–4057; f) B. Blank, M. Colling-Hendelkens, C. Kollann, K. Radacki, D. Rais, K. Uttinger, G. R. Whittell, H. Braunschweig, *Chem. Eur. J.* **2007**, *13*, 4770–4781; g) H. Braunschweig, M. Forster, T. Kupfer, F. Seeler, *Angew. Chem. Int. Ed.* **2008**, *47*, 5981–5983; *Angew. Chem.* **2008**, *120*, 6070–6072; h) G. Alcaraz, U. Helmstedt, E. Clot, L. Vendier, S. Sabo-Etienne, *J. Am. Chem. Soc.* **2008**, *130*, 12878–12879; i) S. Bertsch, H. Braunschweig, B. Christ, M. Forster, K. Schwab, K. Radacki, *Angew. Chem. Int. Ed.* **2010**, *49*, 9517–9520; *Angew. Chem.* **2010**, *122*, 9707–9710.
- [4] a) D. Vidovic, G. A. Pierce, S. Aldridge, *Chem. Commun.* **2009**, 1157–1171; b) H. Braunschweig, R. D. Dewhurst, A. Schneider, *Chem. Rev.* **2010**, *110*, 3924–3957; c) M. Soleilhavoup, G. Bertrand, *Angew. Chem. Int. Ed.* **2017**, *56*, 10282–10292; *Angew. Chem.* **2017**, *129*, 10416–10426.
- [5] a) J. Uddin, G. Frenking, *J. Am. Chem. Soc.* **2001**, *123*, 1683–1693; b) K. K. Pandey, H. Braunschweig, R. D. Dewhurst, *Eur. J. Inorg. Chem.* **2011**, 2045–2056; c) K. K. Pandey, H. Braunschweig, A. Lledos, *Inorg. Chem.* **2011**, *50*, 1402–1410; d) K. K. Pandey, S. Aldridge, *Polyhedron* **2012**, *43*, 131–139; e) G. Frenking, M. Hermann, D. M. Andrada, N. Holzmann, *Chem. Soc. Rev.* **2016**, *45*, 1129–1144.
- [6] P. Pyykkö, *J. Phys. Chem. A* **2015**, *119*, 2326–2337.
- [7] M. J. Drance, J. D. Sears, A. M. Mrse, C. E. Moore, A. L. Rheingold, M. L. Neidig, J. S. Figueroa, *Science* **2019**, *363*, 1203–1205.
- [8] B. Xu, W. Li, W. Yu, Z. Pu, Z. Tan, J. Cheng, X. Wang, L. Andrews, *Inorg. Chem.* **2019**, *58*, 13418–13425.
- [9] T. Jian, L. F. Cheung, T. T. Chen, L. S. Wang, *Angew. Chem. Int. Ed.* **2017**, *56*, 9551–9555; *Angew. Chem.* **2017**, *129*, 9679–9683.
- [10] L. F. Cheung, T. T. Chen, G. S. Kocheril, W. J. Chen, J. Czekner, L. S. Wang, *J. Phys. Chem. Lett.* **2020**, *11*, 659–663.
- [11] M. Peplow, *Chem. Eng. News* **2020**, 98(5), 16.
- [12] C. Chi, J. Q. Wang, H. S. Hu, Y. Y. Zhang, W. L. Li, L. Meng, M. Luo, M. Zhou, J. Li, *Nat. Commun.* **2019**, *10*, 1–6.
- [13] D. Tzeli, A. Mavridis, *J. Chem. Phys.* **2008**, *128*, 034309.
- [14] a) H. J. Zhai, A. N. Alexandrova, K. A. Birch, A. I. Boldyrev, L. S. Wang, *Angew. Chem. Int. Ed.* **2003**, *42*, 6004–6008; *Angew. Chem.* **2003**, *115*, 6186–6190; b) H. J. Zhai, B. Kiran, J. Li, L. S. Wang, *Nat. Mater.* **2003**, *2*, 827–833; c) Z. A. Piazza, H. S. Hu, W. L. Li, Y. F. Zhao, J. Li, L. S. Wang, *Nat. Commun.* **2014**, *5*, 3113; d) A. P. Sergeeva, I. A. Popov, Z. A. Piazza, W. L. Li, C. Romanescu, L. S. Wang, A. I. Boldyrev, *Acc. Chem. Res.* **2014**, *47*, 1349–1358; e) H. J. Zhai, Y. F. Zhao, W. L. Li, Q. Chen, H. Bai, H. S. Hu, Z. A. Piazza, W. J. Tian, H. G. Lu, Y. B. Wu, Y. W. Mu, G. F. Wei, Z. P. Liu, J. Li, S. D. Li, L. S. Wang, *Nat. Chem.* **2014**, *6*, 727–731; f) L. S. Wang, *Int. Rev. Phys. Chem.* **2016**, *35*,

- 69–142; g) A. I. Boldyrev, L. S. Wang, *Phys. Chem. Chem. Phys.* **2016**, *18*, 11589–11605.
- [15] a) C. Romanescu, T. R. Galeev, W. L. Li, A. I. Boldyrev, L. S. Wang, *Angew. Chem. Int. Ed.* **2011**, *50*, 9334–9337; *Angew. Chem.* **2011**, *123*, 9506–9509; b) T. R. Galeev, C. Romanescu, W. L. Li, L. S. Wang, A. I. Boldyrev, *Angew. Chem. Int. Ed.* **2012**, *51*, 2101–2105; *Angew. Chem.* **2012**, *124*, 2143–2147; c) C. Romanescu, T. R. Galeev, W. L. Li, A. I. Boldyrev, L. S. Wang, *Acc. Chem. Res.* **2013**, *46*, 350–358; d) W. L. Li, L. Xie, T. Jian, C. Romanescu, X. Huang, L. S. Wang, *Angew. Chem. Int. Ed.* **2014**, *53*, 1288–1292; *Angew. Chem.* **2014**, *126*, 1312–1316; e) I. A. Popov, T. Jian, G. V. Lopez, A. I. Boldyrev, L. S. Wang, *Nat. Commun.* **2015**, *6*, 8654; f) W. L. Li, T. Jian, X. Chen, T. T. Chen, G. V. Lopez, J. Li, L. S. Wang, *Angew. Chem. Int. Ed.* **2016**, *55*, 7358–7363; *Angew. Chem.* **2016**, *128*, 7484–7489; g) W. L. Li, X. Chen, T. Jian, T. T. Chen, J. Li, L. S. Wang, *Nat. Rev. Chem.* **2017**, *1*, 0071; h) T. T. Chen, W. L. Li, T. Jian, X. Chen, J. Li, L. S. Wang, *Angew. Chem. Int. Ed.* **2017**, *56*, 6916–6920; *Angew. Chem.* **2017**, *129*, 7020–7024; i) W. L. Li, T. T. Chen, D. H. Xing, X. Chen, J. Li, L. S. Wang, *Proc. Natl. Acad. Sci. USA* **2018**, *115*, E6972–E6977; j) T. Jian, X. N. Chen, S. D. Li, A. I. Boldyrev, J. Li, L. S. Wang, *Chem. Soc. Rev.* **2019**, *48*, 3550–3591.
- [16] L. S. Wang, H. S. Cheng, J. Fan, *J. Chem. Phys.* **1995**, *102*, 9480–9493.
- [17] a) G. E. Scuseria, C. L. Janssen, H. F. Schaefer, *J. Chem. Phys.* **1988**, *89*, 7382–7387; b) J. Tao, J. P. Perdew, V. N. Staroverov, G. E. Scuseria, *Phys. Rev. Lett.* **2003**, *91*, 146401.
- [18] D. Figgen, K. A. Peterson, M. Dolg, H. Stoll, *J. Chem. Phys.* **2009**, *130*, 164108.
- [19] R. A. Kendall, T. H. Dunning Jr, R. J. Harrison, *J. Chem. Phys.* **1992**, *96*, 6796–6806.
- [20] M. E. Casida, C. Jamorski, K. C. Casida, D. R. Salahub, *J. Chem. Phys.* **1998**, *108*, 4439–4449.
- [21] A. Kramida, Y. Ralchenko, J. Reader, and NIST ASD Team, NIST Atomic Spectra Database, ver. 5.7.1 (2019). Available online: <https://physics.nist.gov/asd/>.
- [22] D. Y. Zubarev, A. I. Boldyrev, *Phys. Chem. Chem. Phys.* **2008**, *10*, 5207–5217.
- [23] L. F. Cheung, G. S. Kocheril, J. Czekner, L. S. Wang, *J. Chem. Phys.* **2020**, *152*, 174301.
- [24] A. E. Reed, R. B. Weinstock, F. Weinhold, *J. Chem. Phys.* **1985**, *83*, 735–746.
- [25] a) I. Mayer, *Chem. Phys. Lett.* **1983**, *97*, 270–274; b) R. F. Nalewajski, J. Mrozek, A. Michalak, *Int. J. Quantum Chem.* **1997**, *61*, 589–601.
- [26] J. P. Perdew, K. Burke, M. Ernzerhof, *Phys. Rev. Lett.* **1996**, *77*, 3865–3868.
- [27] a) G. te Velde, F. M. Bickelhaupt, E. J. Baerends, C. Fonseca Guerra, S. J. A. van Gisbergen, J. G. Snijders, T. Ziegler, *J. Comput. Chem.* **2001**, *22*, 931–967; b) C. Fonseca Guerra, J. G. Snijders, G. te Velde, E. J. Baerends, *Theo. Chem. Acc.* **1998**, *99*, 391–403; c) ADF2019, SCM, Theoretical Chemistry, Vrije Universiteit, Amsterdam, The Netherlands, <http://www.scm.com>.

Manuscript received: May 7, 2020

Accepted manuscript online: May 18, 2010

Version of record online: June 9, 2020